

Structural optimization for remote white light-emitting diodes with quantum dots and phosphor: packaging sequence matters

BIN XIE,^{1,2} WEI CHEN,² JUNJIE HAO,² DAN WU,³ XINGJIAN YU,¹ YANHUA CHEN,¹ RUN HU,¹ KAI WANG,^{2,4} AND XIAOBING LUO^{1,5}

¹State Key Laboratory of Coal Combustion and Thermal Packaging Laboratory, School of Energy and Power Engineering, Huazhong University of Science and Technology, Wuhan, 430074, China

²Department of Electrical & Electronic Engineering, Southern University of Science and Technology, Shenzhen, 518055, China

³School of Electrical & Electronic Engineering, Nanyang Technological University, Singapore, 639798, Singapore

⁴wangk@sustc.edu.cn

⁵luoxb@hust.edu.cn

Abstract: White light-emitting diodes (WLEDs) with quantum dots (QDs) and phosphor have attracted tremendous attentions due to their excellent color rendering ability. In the packaging process, QDs layer and phosphor-silicone layer tend to be separated to reduce the reabsorption losses, and to maintain the stability of QDs surface ligands. This study investigated the packaging sequence between QDs and phosphor on the optical and thermal performances of WLEDs. The output optical power and PL spectra were measured and analyzed, and the temperature fields were simulated and validated experimentally by infrared thermal imager. It was found that when driven by 60 mA, the QDs-on-phosphor type WLEDs achieved luminous efficiency (LE) of 110 lm/W, with color rendering index (CRI) of $R_a = 92$ and $R_9 = 80$, while the phosphor-on-QDs type WLEDs demonstrated lower LE of 68 lm/W, with $R_a = 57$ and $R_9 = 24$. Moreover, the QDs-on-phosphor type WLEDs generated less heat than that of another, consequently the highest temperature in the QDs-on-phosphor type was lower than another, and the temperature difference can reach 12.3°C. Therefore, in terms of packaging sequence, the QDs-on-phosphor type is an optimal packaging architecture for higher optical efficiency, better color rendering ability and lower device temperature.

© 2016 Optical Society of America

OCIS codes: (250.5590) Quantum-well, -wire and -dot devices; (230.3670) Light-emitting diodes; (310.6845) Thin film devices and applications; (220.2740) Geometric optical design; (120.6810) Thermal effects.

References and links

1. S. Pimpitkar, J. S. Speck, S. P. DenBaars, and S. Nakamura, "Prospects for LED lighting," *Nat. Photonics* **3**(4), 179–181 (2009).
2. X. Luo, R. Hu, S. Liu, and K. Wang, "Heat and fluid flow in high-power LED packaging and applications," *Prog. Energ. Combust.* **56**, 1–32 (2016).
3. H. S. Jang and D. Y. Jeon, "White light emission from blue and near ultraviolet light-emitting diodes precoated with a $\text{Sr}_3\text{SiO}_5:\text{Ce}^{3+}, \text{Li}^+$ phosphor," *Opt. Lett.* **32**(23), 3444–3446 (2007).
4. H. S. Jang, W. B. Im, D. C. Lee, D. Y. Jeon, and S. S. Kim, "Enhancement of red spectral emission intensity of $\text{Y}_3\text{Al}_5\text{O}_{12}:\text{Ce}^{3+}$ phosphor via Pr co-doping and Tb substitution for the application to white LEDs," *J. Lumin.* **126**(2), 371–377 (2007).
5. K. H. Lee and W. B. Im, "Efficiency enhancement of bredigite-structure $\text{Ca}_{14}\text{Mg}_2[\text{SiO}_2]_8:\text{Eu}^{2+}$ phosphor via partial nitridation for solid-state lighting applications," *J. Am. Ceram. Soc.* **96**(2), 503–508 (2013).
6. R.-J. Xie, N. Hirosaki, N. Kimura, K. Sakuma, and M. Mitomo, "2-phosphor-converted white light-emitting diodes using oxynitride/nitride phosphors," *Appl. Phys. Lett.* **90**(19), 191101 (2007).
7. Z. Wang, Z. Xia, M. S. Molokeev, V. V. Atuchin, and Q. Liu, "Blue-shift of Eu^{2+} emission in $(\text{Ba}, \text{Sr})_3\text{Lu}(\text{PO}_4)_3:\text{Eu}^{2+}$ eulytite solid-solution phosphors resulting from release of neighbouring-cation-induced stress," *Dalton Trans.* **43**(44), 16800–16804 (2014).
8. X. Piao, K. Machida, T. Horikawa, H. Hanzawa, Y. Shimomura, and N. Kijima, "Preparation of $\text{CaAlSiN}_3:\text{Eu}^{2+}$ phosphors by the self-propagating high-temperature synthesis and their luminescent properties," *Chem. Mater.* **19**(18), 4592–4599 (2007).

9. K. Uheda, N. Hirotsaki, and H. Yamamoto, "Host lattice materials in the system $\text{Ca}_3\text{N}_2\text{-AlN-Si}_3\text{N}_4$ for white light emitting diode," *Appl. Mater. Sci.* **203**(11), 2712–2717 (2006).
10. K.-S. Cho, E. K. Lee, W.-J. Joo, E. Jang, T.-H. Kim, S. J. Lee, S.-J. Kwon, J. Y. Han, B.-K. Kim, B. L. Choi, and J. M. Kim, "High-performance crosslinked colloidal quantum-dot light-emitting diodes," *Nat. Photonics* **3**(6), 341–345 (2009).
11. Z. Luo, H. Chen, Y. Liu, S. Xu, and S. T. Wu, "Color-tunable light emitting diodes based on quantum dot suspension," *Appl. Opt.* **54**(10), 2845–2850 (2015).
12. K.-J. Chen, Y.-C. Lai, B.-C. Lin, C.-C. Lin, S.-H. Chiu, Z.-Y. Tu, M.-H. Shih, P. Yu, P.-T. Lee, X. Li, H.-F. Meng, G.-C. Chi, T.-M. Chen, and H.-C. Kuo, "Efficient hybrid white light-emitting diodes by organic-inorganic materials at different CCT from 3000K to 9000K," *Opt. Express* **23**(7), A204–A210 (2015).
13. B. Xie, R. Hu, and X. Luo, "Quantum dots-converted light-emitting diodes packaging for lighting and display: status and perspectives," *J. Electron. Packag.* **138**(2), 020803 (2016).
14. T. Erdem, S. Nizamoglu, X. W. Sun, and H. V. Demir, "A photometric investigation of ultra-efficient LEDs with high color rendering index and high luminous efficacy employing nanocrystal quantum dot luminophores," *Opt. Express* **18**(1), 340–347 (2010).
15. J. M. Phillips, M. E. Coltrin, M. H. Crawford, A. J. Fischer, M. R. Krames, R. Mueller-Mach, G. O. Mueller, Y. Ohno, L. E. S. Rohwer, J. A. Simmons, and J. Y. Tsao, "Research challenges to ultra-efficient inorganic solid-state lighting," *Laser Photonics Rev.* **1**(4), 307–333 (2007).
16. P. Zhong, G. He, and M. Zhang, "Optimal spectra of white light-emitting diodes using quantum dot nanophosphors," *Opt. Express* **20**(8), 9122–9134 (2012).
17. Y. Yin, R. Wang, and L. Zhou, "CdTe quantum dots and YAG hybrid phosphors for white light-emitting diodes," *Luminescence* **29**(6), 626–629 (2014).
18. L. Mao, Q. Zhang, Y. Zhang, C. Wang, and S. Chen, "Construction of highly luminescent CdTe/CdS@ZnS-SiO₂ quantum dots as conversion materials toward excellent color-rendering white-light-emitting diodes," *Ind. Eng. Chem. Res.* **53**(43), 16763–16770 (2014).
19. J.-H. Kim, W.-S. Song, and H. Yang, "Color-converting bilayered composite plate of quantum-dot-polymer for high-color rendering white light-emitting diode," *Opt. Lett.* **38**(15), 2885–2888 (2013).
20. J. Y. Woo, K. Kim, S. Jeong, and C.-S. Han, "Enhanced photoluminance of layered quantum dot-phosphor nanocomposites as converting materials for light emitting diodes," *J. Phys. Chem. C* **115**(43), 20945–20952 (2011).
21. H. Qu, L. Cao, G. Su, and W. Liu, "Effect of inorganic shells on luminescence properties of ZnS:Ag nanoparticles," *J. Mater. Sci.* **48**(14), 4952–4961 (2013).
22. N. Reitingner, A. Hohenau, S. Kostler, J. R. Krenn, and A. Leitner, "Radiationless energy transfer in CdSe-ZnS quantum dot aggregates embedded in PMMA," *Phys. Status Solidi., A Appl. Mater. Sci.* **208**(3), 710–714 (2011).
23. C. Yuan, L. Li, B. Duan, B. Xie, Y. Zhu, and X. Luo, "Locally reinforced polymer-based composites for efficient heat dissipation of local heat source," *Int. J. Therm. Sci.* **102**, 202–209 (2016).
24. C. S. Lee, B. Kim, S. Jeon, C. J. Han, and S.-K. Hong, "Thermal curing property of silicone encapsulant containing quantum dot surrounded by various types of ligands," *Bull. Korean Chem. Soc.* **34**(12), 3787–3789 (2013).
25. N. N. Trung, Q.-P. Luu, B. T. Son, L. H. Sinh, and J.-Y. Bae, "Preparation and characterization of silicone resin nanocomposite containing CdSe/ZnS quantum dots," *Polym. Compos.* **33**(10), 1785–1791 (2012).
26. H. Zhang, Z. Cui, Y. Wang, K. Zhang, X. Ji, C. Lu, B. Yang, and M. Gao, "From water-soluble CdTe nanocrystals to fluorescent nanocrystal-polymer transparent composites using polymerizable surfactants," *Adv. Mater.* **15**(10), 777–780 (2003).
27. W. Chen, K. Wang, J. Hao, D. Wu, S. Wang, J. Qin, C. Li, and W. Cao, "Highly efficient and stable luminescence from microbeams integrated with Cd-free quantum dots for white-light-emitting diodes," *Part. Part. Syst. Charact.* **32**(10), 922–927 (2015).
28. J. Y. Woo, K. N. Kim, S. Jeong, and C.-S. Han, "Thermal behavior of a quantum dot nanocomposite as a color converting material and its application to white LED," *Nanotechnology* **21**(49), 495704 (2010).
29. T. Erdem, S. Nizamoglu, and H. V. Demir, "Power conversion and luminous efficiency performance of nanophosphor quantum dots on color-conversion LEDs for quality general lighting," *Proc. SPIE* **8278**, 827811 (2012).
30. L. Yin, Y. Bai, J. Zhou, J. Cao, X. Sun, and J. Zhang, "The thermal stability performances of the color rendering index of white light emitting diodes with the red quantum dots encapsulation," *Opt. Mater.* **42**, 187–192 (2015).
31. J. Y. Woo, K. Kim, S. Jeong, and C.-S. Han, "Enhanced photoluminance of layered quantum dot-phosphor nanocomposites as converting materials for light emitting diodes," *J. Phys. Chem. C* **115**(43), 20945–20952 (2011).
32. J. J. Hao, J. Zhou, and C. Y. Zhang, "A tri-*n*-octylphosphine-assisted successive ionic layer adsorption and reaction method to synthesize multilayered core-shell CdSe-ZnS quantum dots with extremely high quantum yield," *Chem. Commun. (Camb.)* **49**(56), 6346–6348 (2013).
33. W. Chen, K. Wang, J. Hao, D. Wu, J. Qin, D. Dong, J. Deng, Y. Li, Y. Chen, and W. Cao, "High efficiency and color rendering quantum dots white light emitting diodes optimized by luminescent microspheres incorporating," *Nanophotonics* (posted 9 May 2016, in press).

34. R. Hu and X. Luo, "A model for calculating the bidirectional scattering properties of phosphor layer in white light-emitting diodes," *J. Lightwave Technol.* **30**(21), 3376–3380 (2012).
35. Z. Krumer, S. J. Pera, R. J. A. van Dijk-Moes, Y. Zhao, A. F. P. de Brouwer, E. Groeneveld, W. G. J. H. M. van Sark, R. E. I. Schropp, and C. de Mello Donegá, "Tackling self-absorption in luminescent solar concentrators with type-II colloidal quantum dots," *Sol. Energy Mater. Sol. Cells* **110**(0), 57–65 (2013).
36. D. Şahin, B. Ilan, and D. F. Kelley, "Monte-Carlo simulations of light propagation in luminescent solar concentrators based on semiconductor nanoparticles," *J. Appl. Phys.* **110**(3), 033108 (2011).
37. B. Xie, R. Hu, X. Yu, B. Shang, Y. Ma, and X. Luo, "Effect of packaging method on performance of light-emitting diodes with quantum dots phosphor," *IEEE Photonics Technol. Lett.* **28**(10), 1115–1118 (2016).
38. J. H. Kim and M. W. Shin, "Thermal behavior of remote phosphor in light-emitting diode packages," *IEEE Electron Device Lett.* **36**(8), 832–834 (2015).
39. R. Hu, X. Luo, and H. Zheng, "Hotspot location shift in the high-power phosphor-converted white light-emitting diode packages," *Jpn. J. Appl. Phys.* **51**(9S2), 09MK05 (2012).
40. L. Orloff, J. De Ris, and G. H. Markstein, "Upward turbulent fire spread and burning of fuel surface," *Proc. Combust. Inst.* **15**(1), 183–192 (1975).
41. F. Jiang, J. L. de Ris, and M. M. Khan, "Absorption of thermal energy in PMMA by in-depth radiation," *Fire Saf. J.* **44**(1), 106–112 (2009).

1. Introduction

Phosphor converted-light-emitting diodes (pc-LEDs) have been considered as a promising light source in solid-state lighting (SSL) and flat-panel display applications, with their characteristics of high luminous efficiency (LE), low power consumption and long lifetime [1–3]. The most conventional pc-LEDs are realized by combing blue LED chip with yellow emissive $Y_3Al_5O_{12}:Ce^{3+}$ (YAG: Ce) phosphor. Part of the blue light is absorbed by phosphor and converted to yellow light, and the mixture of blue light and yellow light results in white light emission. This type of pc-LEDs can achieve high LE, while their color rendering index (CRI) is rather poor due to the red spectral deficiency [4]. Many attempts have been made to improve the color rendering abilities of pc-LEDs, such as the addition of high efficiency red emissive phosphors [5–8]. However, they are incapable of maintaining high LE because their broad red emission partially lying outside the sensitive region of human eyes [8,9].

Recently, semiconductor quantum dots (QDs) have attracted numerous attentions in SSL applications by virtue of their unique optical properties, such as narrow emission spectra, tunable bandgap and high quantum yields [10–13]. It has been proved theoretically and experimentally that adding QDs into pc-LEDs can greatly improve the CRI and color gamut, and QDs' narrow emission allows for the potential of high LE [14–16]. There are two major packaging strategies for incorporating QDs with pc-LEDs. One is to coat the mixture of QDs and phosphor-silicone gel onto the LED chip to, i.e., the mixed structure [17, 18], and another is to coat QDs layer and phosphor layer separately, i.e., the remote structure [19, 20]. In the mixed type, QDs are filled into the reflection cup and is close to the LED chip. Therefore, the QDs suffer from a high optical power density. While in the remote type, QDs film is away from the chip, thus suffering from a lower optical power density, and the chemical incompatibility between QDs surface ligands and phosphor-silicone gel can be released, by changing the polymeric environment of QDs layer [21–27]. Therefore, the remote packaging structure is widely utilized for fabricating WLEDs with both QDs and phosphor. Figure 1 shows two remote WLEDs with different packaging architecture. In type I (Fig. 1(a)), the QDs layer is coated onto the top of phosphor layer, while in type II (Fig. 1(b)) the phosphor layer is coated onto the QDs layer. The packaging sequence can affect the light output efficiency, consequently changes the temperature distribution, and eventually influences the long-term stability. Although many literatures have discussed the effect of packaging structure on the performance of QDs-WLEDs [28–30], they didn't systematically analyze the optical energy transfer between QDs and phosphor, until Woo et al. [31] firstly compared two kinds of layered structure (QDs-on-phosphor and phosphor-on-QDs) by analyzing the PL decay of QDs and phosphor. Their results provide important guidance for QDs-WLEDs design. However, the optical energy loss of QDs and phosphor in both types have not been

revealed, and the variation of QDs content on the performance variation has not been considered.

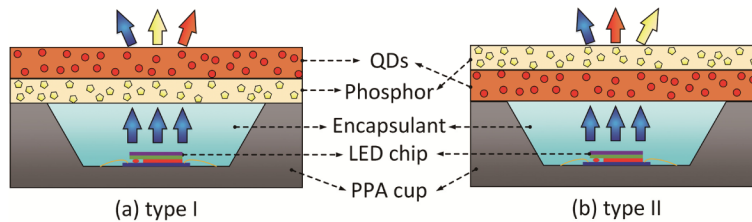


Fig. 1. Schematic showing two remote type WLEDs with different packaging sequences. (a) QDs-on-phosphor type. (b) Phosphor-on-QDs type.

Therefore, in this work, we quantitatively analyzed the performance differences between two types of WLEDs by directly measuring the optical energy loss of QDs and phosphor. The red emissive CdSe/ZnS QDs were synthesized, and WLEDs were fabricated based on YAG:Ce phosphor film and a series of QDs film. The output optical power and PL spectra were measured and analyzed by an integrating sphere system, and the temperature fields were simulated by combing optical measurement with thermal simulation, finally the temperature fields were validated by infrared thermal imager. It was confirmed that in terms of packaging sequence, the QDs-on-phosphor type is an optimal packaging architecture for higher optical efficiency, better color rendering ability and lower device temperature.

2. Preparation, test and simulation methods

2.1 Synthesis of red-emissive CdSe/ZnS core/shell QDs

High quality red-emissive CdSe/ZnS core/shell QDs was prepared by the TOP-assisted SILAR method which had been described in our previous work [32, 33]. For the synthesis of CdSe core, a mixture of 0.4 mmol of CdO and 3.2 mmol of stearic acid in a 50 ml three-neck flask was heated to about 220°C under argon atmosphere to obtain a clear colorless solution. After cooling to room temperature, 50 mmol of octadecylamine (ODA) and 10 ml of octadecene (ODE) were added into the flask, and reheated to 270°C. After the heating device was moved, 4 mmol of Se in 4 ml of TOP was swiftly injected. The growth temperature was then reduced to 250°C for 5 min. Finally, the reaction mixture was cooled to room temperature, and an extraction procedure was used to purify the nanocrystals from side products and unreacted precursors. The obtained CdSe core was dispersed in n-hexane.

For the synthesis of CdSe/ZnS core/shell QDs, red CdSe QDs dissolved in 5 ml of hexanes were mixed with 1.6 g of ODA and 4 ml of ODE in a 50 ml three-neck flask. The flask was applied vacuum to remove hexanes with a mechanical pump at 60°C for 30 min, followed by removing any residual air from the system at 100°C for another 10 min. subsequently, the system was switched to argon atmosphere and the reaction mixture was heated to 140°C for the injections. Then, 0.5 ml of TOP solution was injected as an activator, and the reaction mixture was further maintained at 210°C for 30 min. After the activation, 0.33 ml of Zinc precursor solution (0.1mol/L) was injected and maintained at 200°C for 20 min. Then 0.33 ml of S precursor solution was added. The temperature was increased immediately to 220°C for 60 min to allow in situ growth of the first ZnS monolayer. Cycling of injection and growth continued for the increased monolayers of ZnS shell, for instance, 40 ml of Zinc and S precursors is required for the growth of the second layer, and 48 ml for the third layer. The final product was diluted by hexanes followed by a methanol extraction. The extraction procedure was repeated for three times. The supernatant solution was further purified by centrifugation, and then dissolved in toluene for further use.

2.2 Preparation of WLEDs with QDs and YAG phosphor

Firstly, polymethyl methacrylate (PMMA) was chosen as the polymer matrix of QDs film. The QDs-PMMA film was prepared with in situ polymerization method. 10 ml of MMA monomer and azodiisobutyronitrile (AIBN, 0.2% wt/wt with respect to MMA) were added into a 25 ml three-neck flask and kept stirring until the AIBN was dissolved completely. Subsequently, 20 mg of as-prepared CdSe/ZnS QDs dissolved in toluene was dropwise added into the flask and the mixture was homogeneously dispersed by the ultrasound treatment. After that, the flask was placed into the thermostatic water bath at 70°C for 15 min until the mixture reached certain viscosity, and then cooled to temperature. Then, the viscous liquid was introduced into the tailored mould. The mould was placed in the vacuum oven at 45°C and kept for 24 h. Finally, the resulting film was cut into squares to fit the LED module.

The phosphor-silicone film was prepared by following a typical thermal-curing process. Firstly 0.3 g of YAG phosphor with peak emission wavelength of 550 nm (purchased from InterMatrix) was mixed with 1 g of silicone gel (OE 6550, purchased from Dow Corning). Then the mixture was stirred for 20 min to be dispersed uniformly. Bubbles introduced during the stirring process were removed by applying alternating cycles of vacuum. The resulting composites were then introduced into the tailored mould. Then the mould was placed in the vacuum oven at 150°C and kept for 1 h. Finally the resulting film was cut into squares as well.

WLEDs were fabricated by firstly dispensing the pure silicone gel into the inner space of 2835 SMD LED, and then stacking the QDs layer and/or phosphor film onto the top of LED module, followed by a curing process at 120°C for 30 min. Two WLEDs were prepared and there were five samples for each packaging structure.

2.3 Measurement of heat generation

The optical power of two WLEDs were measured by an integrating sphere (ATA-1000, EVERFINE Inc.), and the heat generation of LED chip, QDs layer and phosphor layer was calculated according to the optical energy losses within the corresponding layer. Figure 2 shows the schematic of the measuring process, and the heat flux of each layer was calculated as follows:

$$P_{heat-chip} = P_{El} - P_{Op-ref} \quad (1)$$

$$P_{heat-phosphor} = P_{Op-ref} - P_{Op-1} - \Psi_{phos} \quad (2)$$

$$P_{heat-QDs} = P_{Op-1} - P_{Op-2} - \Psi_{QDs} \quad (3)$$

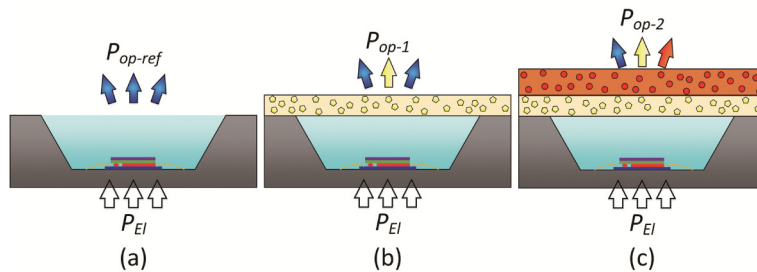


Fig. 2. Schematic showing the measurement process of heat generation in each layer. (a) Measuring the heat flux of LED chip. (b) Measuring the heat flux of phosphor layer. (c) Measuring the heat flux of QDs layer.

Where P_{El} is the input electric power of WLEDs package, P_{Op-ref} is the optical power from LED module with only encapsulant. P_{Op-1} is the optical power from WLEDs packaged with only phosphor layer, Ψ_{phos} is the optical losses derived from part of the backward scattered

light which is absorbed by the inner surface of PPA cup. This is determined by modeling the light absorption, scattering and conversion process in phosphor layer with a modified Kubelka-Munk theory [34]. P_{Op-2} is the optical power from WLEDs packaged with phosphor layer and QDs layer, Ψ_{QDs} is the optical losses derived from part of backward scattered light by QDs particle which is then absorbed by phosphor layer and PPA cup. Herein the heat generation in PPA cup is negligible due to its high reflectance and low absorption, and scattering coefficient of QDs is assumed to be zero due to their small size [35, 36]. Therefore, Ψ_{QDs} and Ψ_{phos} are zero in the thermal simulation. Besides, it is assumed that the entire optical power loss is converted into heat in each layer [37, 38]. These assumptions are proposed from experiments, and have been proved reasonable in many literatures.

2.4 Thermal simulation setup

To conduct the thermal simulations, we built the corresponding physical model of two types of WLEDs, as shown in Fig. 3. The WLEDs were mounted on a metal-core printed circuit board (MCPCB) for electrical connection and heat dissipation. Thickness and thermal conductivity of each layer used in the simulation is listed in Table 1. Herein the thermal conductivity of phosphor layer and QDs layer are calculated based on a weighted average between polymer matrix and fluorescent particles. The heat flux of LED chip, QDs layer and phosphor layer were loaded on the physical model and then the thermal simulations were conducted with finite element method (FEM).

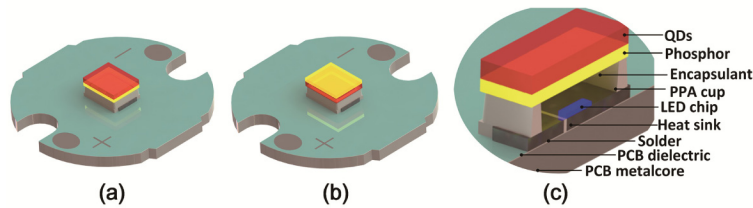


Fig. 3. Physical model of the as-prepared WLEDs. (a) WLEDs with QDs-on-phosphor structure (type I). (b) WLEDs with phosphor-on-QDs structure (type II). (c) FEM simulation model of the WLEDs.

Table 1. Thickness and thermal conductivity of the packaging materials used in the thermal simulation

Material	Thickness (mm)	Thermal Conductivity (W/m·K)
PCB Metalcore	0.98	170
PCB Dielectric	0.02	0.2
Solder	0.05	5
Heat Sink	0.3	170
LED Chip	0.1	65.6
PPA Cup	0.8	0.36
Encapsulant	0.8	0.175
Phosphor Layer	0.3	0.18
QDs Layer	0.44	0.16

In the FEM simulation, only a half of the WLEDs model was utilized to simulate the temperature field, due to its symmetry. The boundary conditions of the FEM model were set as follows: the ambient temperature was fixed at 24°C; natural convection occurred at the bottom surface of the PCB with a heat transfer coefficient of 10 W/(m²·K), and other surfaces are cooled by natural convection with a heat transfer coefficient of 8 W/(m²·K). All the boundary conditions were similar as those in [39].

3. Results and discussions

Figure 4(a) depicts the high resolution transmission electron microscope (HRTEM) images of the as-prepared CdSe/ZnS core-shell QDs, suggesting the average diameter of QDs are 6.8 nm with uniform size distribution. Figure 4(b) illustrates the absorption and PL spectra of the as-prepared CdSe core and CdSe/ZnS core-shell QDs. The apparent first exciton peaks from absorption spectra and narrow full width at half maximum (FWHM) of near 31 nm from PL spectra have confirmed the uniform size distribution of as-prepared QDs. Benefited from the TOP-assisted SILAR method, which remove the surface lattice imperfections by the surface ions re-dissolution and lattice re-arrangement during the whole ZnS shell formation process, the absolute PL quantum yields (PLQY) was enhanced efficiently from 45% (core) to 69% (core-shell), as depicted in Fig. 4(b). Figures 4(c) and 4(d) show the photographs of the phosphor film and QDs film under daylight and UV light, respectively. It is seen that both films maintained high transparency and uniformity. The thickness of phosphor film and QDs film was measured as 0.3 mm and 0.44 mm, respectively.

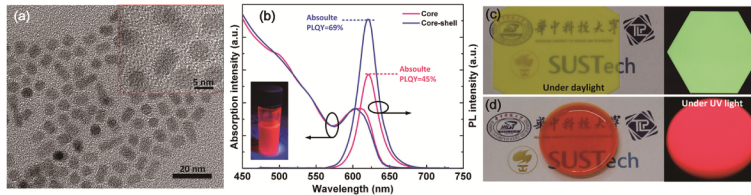


Fig. 4. (a) HRTEM images of the as-prepared CdSe/ZnS core-shell QDs. (b) Absorption and PL spectra of the CdSe core and CdSe/ZnS core-shell QDs, the inset in Fig. 4(b) shows the CdSe/ZnS QDs solution under UV light exposure. (c) Photographs of the as-prepared phosphor film under daylight and UV light. (d) Photographs of the as-prepared QDs film under daylight and UV light.

Figure 5 shows the current-dependent heat generation in type I and type II WLEDs. It is illustrated that in type I, the heat flux of LED chip is much larger than that of phosphor layer and QDs layer. The heat generation in phosphor layer is close to that in QDs layer, and their heat flux increased with the increasing driving current. For instance, in the rated driving current of 60 mA, the heat flux of LED chip, phosphor layer and QDs layer is 81.14 mW, 20.15 mW and 14.82 mW, respectively. However, the heat generation in type II is quite different from type I. Although the majority of heat flux is still generated from LED chip, the heat flux of QDs layer is larger than that of phosphor layer. At driving current of 60 mA, the heat flux of phosphor layer and QDs layer is 8.7 mW and 41.04 mW, respectively. Moreover, as driving current increases, the QDs heat flux increases evidently while the phosphor heat flux barely changes.

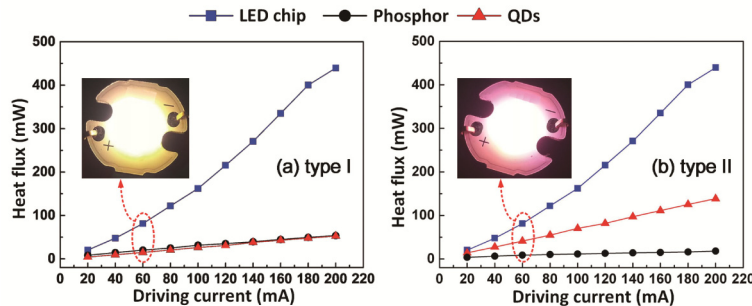


Fig. 5. Heat flux of each layer in type I (a) and type II (b) WLEDs at varying driving current from 20 mA to 200 mA. Inset in (a) and (b) shows the corresponding photograph of WLEDs illuminated at 60 mA.

The difference of heat generation in these two types of WLEDs can be explained from their spectral power distribution, as depicted in Fig. 6. In type I (Fig. 6(a)), blue light rays were emitted from LED chip and firstly incident into phosphor layer. During this process, part of blue light was absorbed by phosphor particle and partly converted into yellow light. For instance, when driven by 60 mA, 70.6 mW of blue light energy was absorbed by phosphor layer and 51.7 mW of yellow light energy was generated, indicating that the conversion efficiency of the phosphor film is 73.2%. Then transmitted blue light rays and converted yellow light rays incident into QDs layer. During this process, part of blue and yellow light was absorbed by QDs particle and then partly converted into red light. Consequently, the mixture of blue, yellow and red light results in white color with LE = 110 lm/W, CCT = 3770 K and excellent color rendering ability of Ra = 92 and R9 = 80.

However, in type II (Fig. 6(b)), blue light rays firstly incident into QDs layer. During this process, 62.8 mW of blue light power was absorbed by QDs layer and 30.5 mW of red light power was generated, which indicates that the conversion efficiency of the QDs film is 48.6%. Due to the lower conversion efficiency of QDs film than phosphor layer, this process generates more heat than that in type I. After that, transmitted blue light rays and converted red light rays incident into phosphor layer. During this process, only part of blue light was absorbed by phosphor and then partly converted into yellow light, the QDs emission light cannot be absorbed by phosphor because QDs emission wavelength lies beyond the absorption spectra of yellow phosphor. Therefore, there is less yellow composition and too much red composition in the PL spectra of type II WLEDs, resulting in an extremely warm color of CCT = 2185 K with LE = 68 lm/W and poor color rendering ability of Ra = 57 and R9 = 24, at driving current of 60 mA.

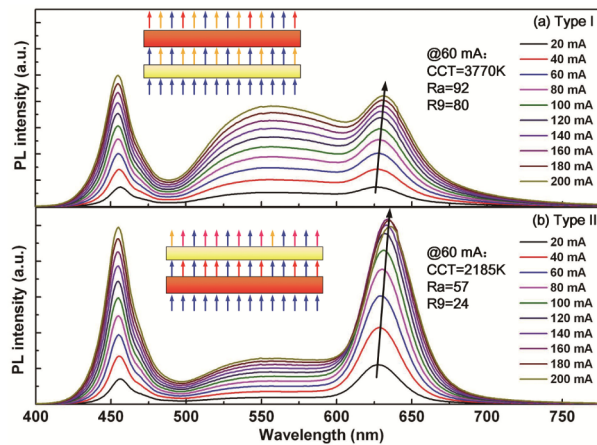


Fig. 6. PL spectra of type I (a) and type II (b) WLEDs under various forward currents ranging from 20 mA to 200 mA. The inset in each figure depicts the corresponding schematic of light output and conversion mechanism.

To investigate the temperature effect of two types of WLEDs, the measured heat flux was loaded on the FEM model and thermal simulations were performed. Figure 7 shows the temperature fields of these WLEDs under driving current of 20 mA and 60 mA. It is seen that the highest temperature of all these WLEDs locates in the top film, which implies that the film temperature is higher than chip temperature in the remote type WLEDs package. This may attribute to the low thermal conductivity of QDs layer and phosphor layer. Moreover, the highest temperature in type I is lower than that in type II, and this difference is more apparent at larger driving current. For example, when driven by 60 mA, the highest temperature in type I is 9.3°C lower than that in type II.

The corresponding temperature fields of the two WLEDs were measured to validate the simulation results. Infrared thermal imager (FLUKE Ti10) was used to obtain the temperature distribution. The emissivities of phosphor and QDs films are set as 0.96 and 0.92 [40, 41], respectively. The distance between camera lens and WLEDs is 0.5 m. Figure 8 gives the measured steady-state temperature fields. It is seen that the simulated temperature distributions between these two WLEDs agree well with the experiments, and the relative error of the highest temperature between experimental and simulation results is less than 2.8%. Therefore, it was confirmed by the experimental data that the highest film temperature in type II is higher than that in type I, the temperature difference is 12.3°C at driving current of 60 mA. Considering the similar thermal conductivity of QDs layer and phosphor layer, the higher temperature in type II is mainly attributes to its higher heat generation.

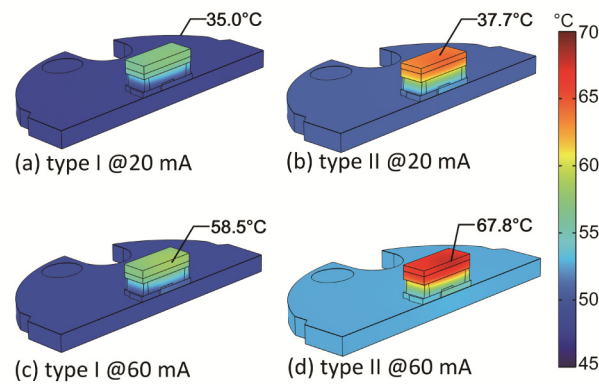


Fig. 7. Simulated steady-state temperature fields of the two WLEDs under driving current of 20 mA and 60 mA. (a) Type I at 20 mA. (b) Type II at 20 mA. (c) Type I at 60 mA. (d) Type II at 60 mA.

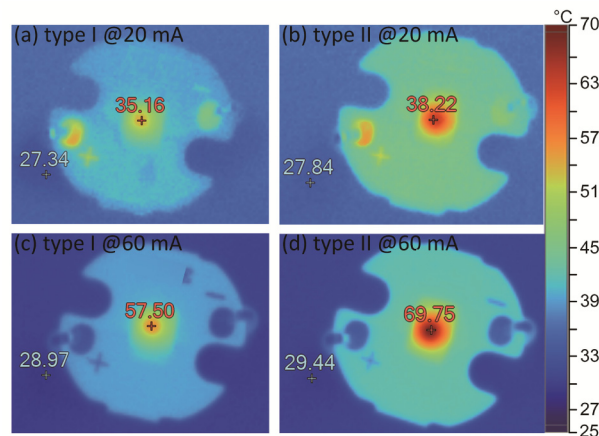


Fig. 8. Temperature fields of the two WLEDs measured by infrared thermal imager. (a) Type I at 20 mA. (b) Type II at 20 mA. (c) Type I at 60 mA. (d) Type II at 60 mA.

To further analyze the performance differences between Type I and Type II, three QDs films with the same thickness but varying QDs concentration were prepared, and the corresponding Type I and Type II WLEDs were fabricated. The three QDs films were prepared by adding 15 mg, 10 mg, 5 mg QDs into 10 mL of PMMA mixture, respectively. The corresponding WLEDs were labeled as S2, S3 and S4, and the previous WLEDs were labeled as S1.

Figure 9 shows the PL spectra of the as-prepared S2-S4 WLEDs illuminated by 60 mA. It is seen that with the QDs concentration decreasing, the CRI of Type I WLEDs decreased correspondingly, while that of Type II varied non-monotonously. This is because the QDs film is located on the top of the device in Type I, thus the variation of QDs concentration mainly leads to the change of red-emission. While in Type II, the change of QDs concentration will change the yellow- and red-emission simultaneously, thus causing the non-monotonous change of color rendering properties. Therefore, Type I is more suitable for tuning the CRI of WLEDs. It can be also found that with the decrease of QDs concentration, the CCT and LE in both types increased, while Type I still has advantage in energy efficiency than Type II.

Figure 10 gives the steady-state thermal images of these six WLEDs under driving current of 60 mA. The peak temperature in Type II is higher than that in Type I, which confirms that more light energy is converted into heat in Type II. Meanwhile, the peak temperature difference between these two types is reduced with the reducing QDs concentration. For instance, the peak temperature difference in S2 samples is 6.7 °C, and that in S4 samples is 2.9 °C. It can be deduced that in extreme case of which QDs concentration is 0, these two types will reach an equal peak temperature.

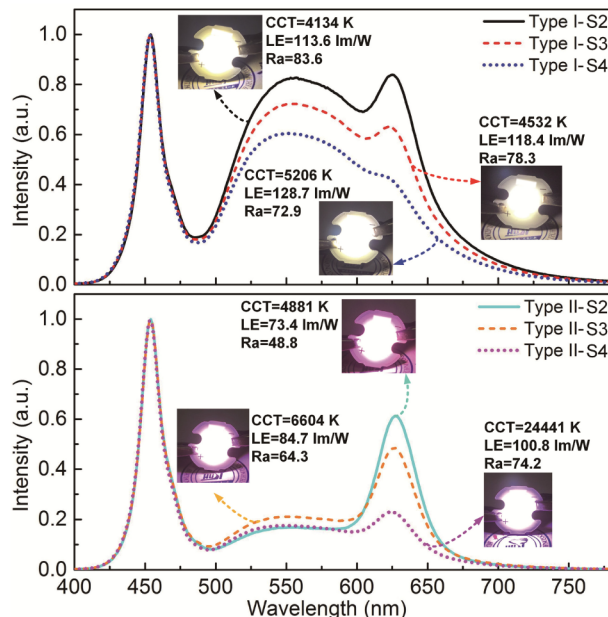


Fig. 9. PL spectra of the fabricated S2-S4 WLEDs under driving current of 60 mA.

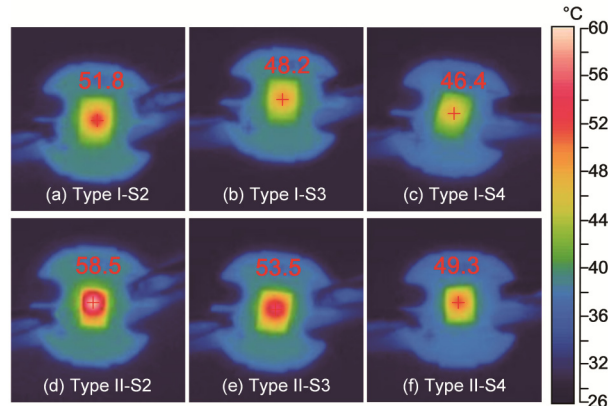


Fig. 10. Measured temperature fields the fabricated S2-S4 WLEDs under driving current of 60 mA. (a) Type I-S2. (b) Type I-S3. (c) Type I-S4. (d) Type II-S2. (e) Type II-S3. (f) Type II-S4.

To sum up, the QDs-on-phosphor type could achieve high CRI and LE than the phosphor-on-QDs type, and could maintain a lower device temperature, which is beneficial for the long-term reliability of WLEDs. Although the temperature difference between these two types can be reduced by reducing the QDs concentration, Type II is not suitable for tuning the color rendering properties of WLEDs. It is noteworthy that the advantages of Type I is revealed in terms of packaging sequence, while when realized the same spectral distribution (i.e., the same CCT), whether the QDs-on-phosphor type can achieve a better optical and temperature performance needs further investigation.

4. Summary and conclusion

This study quantitatively analyzed the optical and thermal performances of two types of remote WLEDs with different packaging sequence. The output optical power and PL spectra were measured and analyzed by an integrating sphere system, and the temperature fields were simulated by combing optical measurement with thermal simulation, finally the temperature fields were validated by infrared thermal imager. It was found that when driven by 60 mA, the QDs-on-phosphor type WLEDs achieved LE of 110 lm/W, with color rendering index (CRI) of $R_a = 92$ and $R_9 = 80$, while the phosphor-on-QDs type WLEDs demonstrated lower LE of 68 lm/W, with $R_a = 57$ and $R_9 = 24$. Moreover, the QDs-on-phosphor type WLEDs generated less heat than that of another, consequently the highest temperature in the QDs-on-phosphor type was lower than another, and the temperature difference can reach 12.3°C. Therefore, in terms of packaging sequence, the QDs-on-phosphor type is an optimal packaging architecture for higher optical efficiency, better color rendering ability and lower device temperature.

Funding

National Science Foundation of China (51576078, 51376070, 51402148); Shenzhen Innovation Project (KC2014JSQN0011A, KQCX20140522151322950).

Acknowledgments

The authors would like to thank Tianjin Zhonghuan Quantum Tech Co., Ltd. for the technical supports with the fabrication of WLEDs.